RSC Advances

ROYAL SOCIETY OF CHEMISTRY

www.rsc.org/advances

RSC Advances

RSCPublishing

ARTICLE

Theoretical Study on the Structural, Electronic and Physical Properties of Layered Alkaline-Earth-Group-4 Transition-Metal Nitrides $AEMN_2$

Cite this: DOI: 10.1039/x0xx00000x

Received 00th May 2014,
Accepted 00th May 2014

DOI: 10.1039/x0xx00000x

www.rsc.org/

Esther Orisakwe,[a] Bruno Fontaine,[a] Duncan H. Gregory,[b] Régis Gautier,*[,a] and Jean-François Halet*[,a]

Thermodynamic, structural, and electronic properties of the layered ternary nitrides $AEMN_2$ (AE = alkaline-earth; M = Group 4 transition metal) both with the $KCoO_2$ and α-$NaFeO_2$ structure-types are examined within density-functional theory. The AE:M atomic (or ionic) radius ratio seems to be the most important criterion in determining one structural arrangement over the other. We find that the majority of compounds is more stable with the $KCoO_2$ structure-type where M is coordinated to five nitrogen atoms in a distorted square-based pyramidal geometry. Strong interactions occur in both arrangements not only between nitrogen and transition metal atoms, but also between nitrogen and alkaline-earth metal atoms within and between the layers. Calculations show that all the $AEMN_2$ compounds with the tetragonal structure-type $KCoO_2$ are semiconducting with band gaps of approximately 1 eV. However, small band gap conductor and even semi-metallic behavior are computed for compounds with the alternative hexagonal α-$NaFeO_2$ structure-type.

Introduction

The solid-state chemistry of ternary nitridometalates has rapidly emerged and matured in recent years, both in the context of their many varied physical properties and of their potentially useful applications.[1-14] These compounds display a wide range of varying and often unique crystal structures in which the metals – often transition metals – exhibit unusual oxidation states and/or coordination to nitrogen. Examples include the families of the ternary phases AE_3MN_3 (AE = alkaline earth metal; M = V, Cr, Mn, Fe)[15-17] and Ca_6MN_5 (M = Fe, Ga, Mn),[18,19] with structures unique to nitrides in which M^{3+} cations are coordinated to three nitrogen atoms to form sheets of carbonate-like $[MN_3]^{6-}$ trigonal planar units separated by AE cations. Ternary nitridometalates can also adopt structure types encountered in oxide and carbide chemistry. CaNiN for instance adopts the YCoC structure and contains infinite chains of linear $[NiN]^{2-}$ units,[20] whereas Ba_2VN_3 crystallizes in the Rb_2TiO_3 structure with chains of corner-sharing $[VN_3]^{4-}$ tetrahedra.[21] Another important family of ternary nitridometalates is that of AMN_2 compounds, which adopt structure types found in oxide and chalcogenide chemistry. A subset of these compounds, which embrace both alkali (alkaline-earth) metal-group 6 (group 5) transition metal and mixed transition metal systems, are layered compounds containing metal atoms coordinated by nitrogen in either octahedral or trigonal prismatic geometry.[6,8,22] The $LiMN_2$ compounds (M = Mo, W) were the first metallic layered lithium ternary nitrides to be discovered.[22] They are hexagonal layered compounds of structure type P3 (isotructural with $Na_{0.6}CoO_2$, space group $R3$, No. 146) in which the Mo or W atoms are octahedrally surrounded by nitrogen atoms which themselves sit in a trigonal prismatic environment. The Li^+ cations are located in trigonal prismatic holes between the $[MoN_2]^-$ (or $[WN_2]^-$) layers. These metallic layered compounds are also paramagnetic in character.[23] The mixed transition metal compound $CrWN_2$ is isostructural to $LiMoN_2$ with alternating layers of tungsten and chromium in a trigonal prismatic and octahedral coordination respectively with nitrogen.[24] $CaMN_2$, (M = Nb, Ta)[22] and $SrMN_2$ (M = Zr, Hf)[25] adopt another layered arrangement; the α-$NaFeO_2$ structure-type (hexagonal space group R-3, No. 166 with Z = 3). This arrangement, depicted in Figure 1 for $SrZrN_2$, differs from the P3 structure in that the s-block metal cations are *octahedrally* coordinated by nitrogen. Interestingly, a certain number of $AEMN_2$ compounds (where M is a group 4 metal) including $BaHf_{1-x}Zr_xN_2$ (x = 0-1)[26] and

$SrTiN_2$ (Figure 2)[27,28] are isotypic with the $KCoO_2$ structure type (tetragonal space group *P*4/*nmm*, No. 129, *Z* = 2). Unlike the hexagonal P3 and α-$NaFeO_2$ compounds above, the transition metal atoms in the $KCoO_2$-type are coordinated by five nitrogen atoms in a distorted square-based pyramidal geometry (with four long basal *M*-N bonds and one short apical *M*-N bond), forming layers of edge-sharing pyramids, which stack along the *c* direction. The alkaline-earth atoms *AE* are situated between the $[MN_2]^{2-}$ layers and are also surrounded by five nitrogen atoms in a square-pyramidal arrangement.

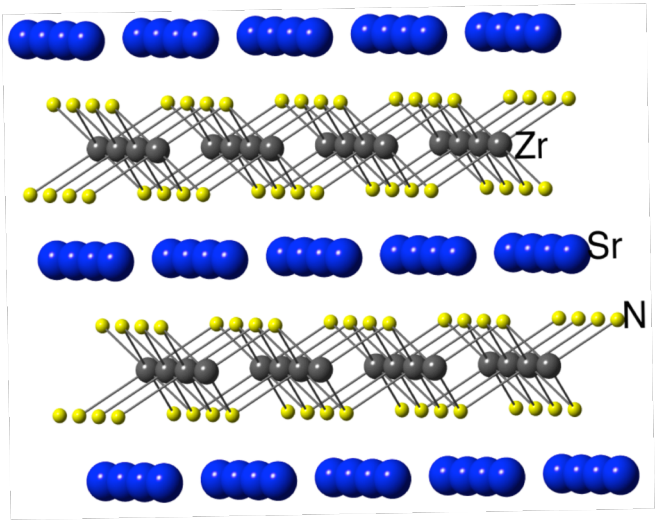

Figure 1. Crystal structure of $SrZrN_2$ (with the α-$NaFeO_2$ structure-type). Large blue, medium grey and small yellow spheres represent Sr, Zr and N atoms, respectively.

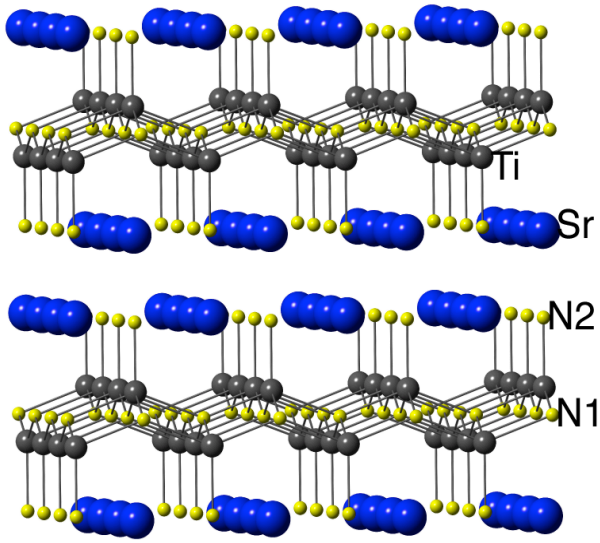

Figure 2. Crystal structure of $SrTiN_2$ (with the $KCoO_2$ structure-type). Large blue, medium grey and small yellow spheres represent Sr, Ti and N atoms, respectively. The unit cell contains two independent nitrogen atoms (N1 (¾, ¼, ½) and N2 (¼, ¼, z)).

Surprisingly, with the usual nominal oxidation states of 3- and 2+ for N and the *AE* metals respectively, the formal *d*-electron count for the Group 4 transition metal in the above *AEM*N_2 compounds is d^0, irrespective of whether the α-$NaFeO_2$ or $KCoO_2$ structure is adopted. A glance at Table 1,[29] which contains both the existing and as-yet unknown *AEM*N_2 compounds, seems to suggest that both the electron count *and* the *AE*:*M* radius ratio govern the preferred structural arrangement.

Theoretical studies have been performed previously on some of the compounds given in Table 1 but these are few in number and much remains to be understood. The unexpected magnetic properties of $SrTiN_2$ were tentatively elucidated.[28] Electronic and vibrational properties of $BaHfN_2$ were studied showing semiconducting behavior with an indirect band gap.[30] However, no comprehensive study has yet been performed to rationalize the observed structures, bonding and physical properties in these *AEM*N_2 compounds. This is the modest ambition of this paper using density-functional theory (DFT) calculations.

Table1. Relation between the experimentally observed structures and the *AE*:*M* atomic and ionic (in brackets) radius ratio for the *AEM*N_2 compounds studied.[29]

	Ti	Zr	Hf
Ca	1.29 (1.46)	1.16 (1.24)	1.16 (1.43)
Sr	1.43 (1.66)	1.29 (1.41)	1.29 (1.55)
Ba	1.54 (1.99)	1.39 (1.69)	1.39 (1.75)

Structure $KCoO_2$
Structure α-$NaFeO_2$
Uncharacterized

Results and Discussion

Thermodynamics and Structure

Relative energies for the different *AEM*N_2 compounds in the two structure-types are compared in Figure 3. Among the 9 compounds considered, 6 are computed to be thermodynamically more stable with the $KCoO_2$ tetragonal structural arrangement. This is in agreement with experiment in the case of $SrTiN_2$, $BaZrN_2$ and $BaHfN_2$.[26, 27, 31] In fact, it is apparent that all Ba compounds would prefer to adopt the $KCoO_2$ structure since the hypothetical compound $BaTiN_2$ is computed to be more thermodynamically stable when adopting the $KCoO_2$ structure than with the α-$NaFeO_2$ alternative by an appreciable margin. $SrZrN_2$ is computed to be slightly more stable (*ca.* 0.1 eV/formula unit (f. u.)) with the $KCoO_2$ structure, contrary to experiment, which demonstrates that the α-$NaFeO_2$ structure is formed by the nitridozirconate.[25] The computational result may suggest that both arrangements could be observed experimentally under appropriate synthetic conditions. $SrHfN_2$ is computed to be more stable with the α-$NaFeO_2$ structure, as is observed experimentally,[25] but the $KCoO_2$ is predicted to be only 0.2 eV/f.u. less stable. No group 4 transition metal Ca*M*N_2 compounds have been reported so far. Calculations indicate that these hypothetical nitrides would

preferentially crystallize in the α-$NaFeO_2$ structure. This is especially true for $CaZrN_2$ and $CaHfN_2$ where the difference in thermodynamic stability with the $KCoO_2$ structure type is large. Given that all the above $AEMN_2$ compounds are isoelectronic, we can postulate that the *AE*:*M* atomic (or ionic) radius ratio may play a deciding role in imposing one structure over the other. Although the total number of characterized compounds is not large, it seems that for an *AE*:*M* atomic radius ratio of around 1.3, the α-$NaFeO_2$ structure type will be preferred, whereas with a ratio of approximately 1.4, the $KCoO_2$ structure prevails. On this basis, $CaTiN_2$ should be observed with the α-$NaFeO_2$ structure type, although, calculations indicate a very small thermodynamic preference for the $KCoO_2$ structure.

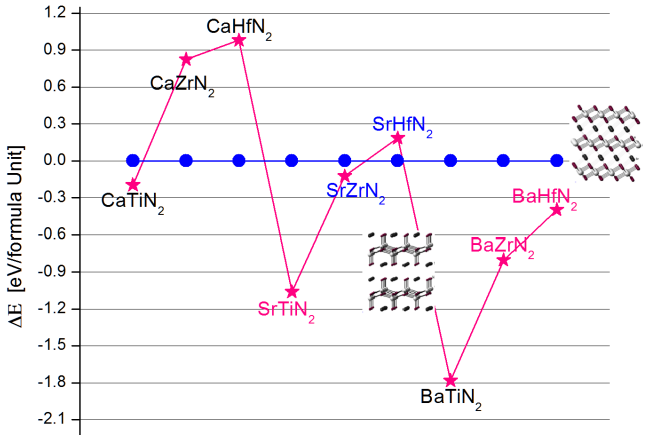

Figure 3. Relative energy difference between $KCoO_2$ (pink) and α-$NaFeO_2$ (blue) structure types for $AEMN_2$ compounds. Compounds with formulae in red and blue experimentally adopt the $KCoO_2$ and α-$NaFeO_2$ structure types, whereas those in black have yet to be discovered.

Tables 2 and 3 summarize the cell parameters, cell volumes, bulk moduli, and pertinent interatomic distances obtained from geometry optimization of the nine $AEMN_2$ compounds in each of the α-$NaFeO_2$ and $KCoO_2$ structure types, respectively. Existing experimental and computational data are included for comparison where available. The good agreement between the computed and experimental structures (deviation < 2% overall) inspires confidence in the prediction of structures for those compounds that have yet to be synthesized and characterized. As expected, for a given *AE* element, a significant increase in both *a* and *c* parameters is computed on moving from Ti to Zr and Hf compounds leading to an expansion of more than 12% in the unit cell volumes for the α-$NaFeO_2$ structures. For *AE* = Ca and Sr, this increase is even larger for compounds adopting the $KCoO_2$ structure type (*ca.* 20% vs. *ca.* 13% for $BaMN_2$ compounds).

It is noteworthy that *M*-N distances differ substantially in α-$NaFeO_2$ and $KCoO_2$ structure types. Six rather long *M*-N distances are encountered around the octahedrally coordinated metal in the former, whereas four shorter (5-8%) *M*-N_{basal} contacts and a significantly shorter (by 12-15%) M-N_{apical} contact are computed for the latter.

Resistance to volume change was analyzed by computing the bulk modulus, *i.e.* the second derivative of the total energy with respect to the volume, for all $AEMN_2$ compounds. Values reported in Tables 2 and 3 show that compounds with the α-$NaFeO_2$ structure-type are less compressible than those with the $KCoO_2$ structure-type. This is particularly the case for the hypothetical $CaMN_2$ compounds with the former structure-type, the bulk moduli of which are computed to be comparable to that of steel and *ca.* 30% larger than compounds with the $KCoO_2$ structure-type.

Electronic and Physical Properties

Band structures and the partial and total density of states (PDOS and DOS) of the different $AEMN_2$ compounds were examined in order to gain insight regarding their electronic properties. For brevity, we will limit our discussion to the electronic structure of $SrTiN_2$ as a representative example of the series.

The calculated PDOS and DOS of $SrTiN_2$ when adopting the experimentally observed $KCoO_2$ structure type are depicted in Figure 4. The total DOS divides into three main regions. The first is located between -15 and -10 eV and is derived from the N 2s orbitals. The second region that is centered close to -2.5 eV below the Fermi level (e_F), is somewhat broader and is mostly due to N 2p N orbitals with a substantial admixture of Sr and Ti valence (mostly *d*-type) orbitals. Interestingly, PDOS for basal N1 and apical N2 atoms differ slightly, with those of the former being broader and lying at somewhat lower energy than those of the latter. The large DOS above the Fermi level shows the dominance of the Ti orbitals, which are combined to a small extent with Sr and N orbitals. The metal orbital participation in the valence band in the vicinity of ε_F, coupled with the nitrogen orbital contribution to the conduction band which is otherwise predominantly comprised of metal states reflect the rather strong metal-nitrogen covalent interactions. Contrary to previous LMTO results,[28] $SrTiN_2$ is computed to be diamagnetic. The simplified description of the Kohn-Sham potential in the LMTO method may be at the origin of this discrepancy.

RSC Advances

RSCPublishing

ARTICLE

Table 2. DFT optimized (normal type) and experimental (*italics*) cell parameters, *AE*-N and *M*-N bond distances, unit cell volume V, bulk modulus B_0, and band gap of *AEM*N_2 compounds adopting the α-$NaFeO_2$ Structure.

Structure	*a* / Å	*c* / Å	A-N / Å	M-N/ Å	V / Å^3	B_0 / GPa	Band Gap / eV	Ref.
$CaTiN_2$	3.138	16.404	2.424	2.132	139.9	173	0	
$CaZrN_2$	3.318	16.843	2.494	2.266	160.6	161	0.45	
$CaHfN_2$	3.292	16.811	2.486	2.247	157.8	171	0.45	
$SrTiN_2$	3.211	17.335	2.571	2.159	154.8	139	0	
$SrZrN_2$	3.382	17.781	2.629	2.281	176.1	129	0.40	
	3.373	*17.676*	*2.609*	*2.292*	*174.1*			[25]
$SrHfN_2$	3.353	17.684	2.607	2.277	172.2	166	0.40	
	3.345	*17.678*	*2.602*	*2.273*	*171.3*			[25]
$BaTiN_2$	3.279	18.451	2.749	2.181	171.8	115	0	
$BaZrN_2$	3.446	18.921	2.818	2.302	194.6	123	0	
$BaHfN_2$	3.418	18.888	2.806	2.286	191.1	122	0	

Table 3. DFT optimized (normal type) and experimental (*italics*) cell parameters, *AE*-N and *M*-N bond distances, unit cell volume V, bulk modulus B_0, and band gap of *AEM*N_2 compounds adopting the $KCoO_2$ Structure.

Structure	*a* / Å	*c* / Å	A-N / Å	M-N/ Å	V / Å^3	B_0 / GPa	Band Gap / eV	Ref.
$CaTiN_2$	3.807	7.517	2.253 (× 1) 2.694 (× 4)	1.844 (× 1) 2.024 (× 4)	108.9	127	1.00	
$CaZrN_2$	3.996	8.131	2.471 (× 1) 2.826 (× 4)	2.009 (× 1) 2.160 (× 4)	129.8	130	1.60	
$CaHfN_2$	3.960	8.150	2.306 (× 1) 2.807 (× 4)	2.016 (× 1) 2.138 (× 4)	127.8	128	1.70	
$SrTiN_2$	3.802	7.776	2.596 (× 1) 2.691 (× 4)	1.836 (× 1) 2.056 (× 4)	112.4	123	0.80	
	3.882	*7.701*	*2.611 (× 1)* *2.747 (× 4)*	*1.827 (× 1)* *2.053 (× 4)*	*116.1*			[28]
	3.880	*7.699*	*2.581 (× 1)* *2.745 (× 4)*	*1.839 (× 1)* *2.056 (× 4)*	*115.9*			[27]
$SrZrN_2$	4.069	8.296	2.523 (× 1) 2.882 (× 4)	2.018 (× 1) 2.179 (× 4)	137.3	122	1.15	
$SrHfN_2$	4.043	8.278	2.539 (× 1) 2.865 (× 4)	2.008 (× 1) 2.162 (× 4)	135.3	123	1.20	
$BaTiN_2$	4.014	8.068	2.856 (× 1) 2.939 (× 4)	1.827 (× 1) 2.106 (× 4)	130.0	101	0.80	
$BaZrN_2$	4.188	8.502	2.858 (× 1) 2.932 (× 4)	2.000 (× 1) 2.228 (× 4)	149.1	124	1.10	
	4.161	*8.392*	*2.771 (× 1)* *2.948 (× 4)*	*2.011 (× 1)* *2.202 (× 4)*	*145.3*			[26]
$BaHfN_2$	4.152	8.491	2.819 (× 1) 2.946 (× 4)	1.993 (× 1) 2.198 (× 4)	146.4	106	1.10	
	4.128	*8.382*	*2.680 (× 1)* *2.922 (× 4)*	*2.050 (× 1)* *2.186 (× 4)*	*142.8*		*[0.95–1.25]*[a]	[26]

[a]Reference 30 - Range of band gaps values obtained from PBE calculations using different pseudopotentials.

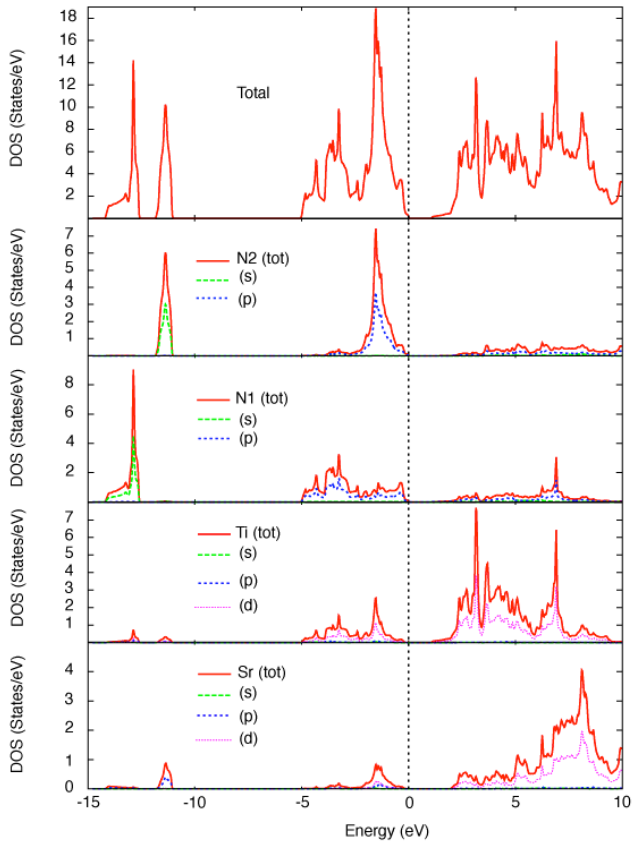

Figure 4. PDOS and DOS of $SrTiN_2$ with the $KCoO_2$ structure-type. The Fermi energy level is set at 0 eV.

The band structure shown in Figure 5 indicates a semiconducting behavior with a calculated (direct) band gap of *ca*. 0.8 eV. Since LDA and GGA functionals usually underestimate band gaps, the true band gap is likely to be larger than 1 eV. For comparison, all the computed band gaps for the compounds with the $KCoO_2$ structure are given in Table 3. The small dispersion of bands in Γ→Z and A→M show the weak interaction between MN_2 nets. The lowest conduction band has primarily Ti $3d_{xy}$ character. The large dispersion of this band is due to Ti-Ti interactions within the layers. The band structure sketched in Figure 5 agrees with a recent theoretical study carried out for some of these nitrides in order to evaluate their thermoelectric performance.[32]

Total and partial DOS for $SrTiN_2$ in the alternative α-$NaFeO_2$ structure-type are shown in Figure 6. As is the case for the $KCoO_2$ structure-type, the total DOS also divides into three main regions but the low lying band is notably narrower for the α-$NaFeO_2$ structure. The valence band is once more dominated by N 2s and 2 p orbitals with some contribution from the metal atoms, whereas the conduction band derives mostly from the metal orbitals with some admixture of N orbitals. It is noteworthy that the tails of the valence and conduction bands are in contact at the Fermi level. This semi-metallic character is confirmed by an analysis of the band structure shown in Figure 7. It is important to note that the (indirect) band gap is computed as almost 0.6 eV using the mBJ functional proposed by Tran and Blaha that yields band gaps with accuracy similar to hybrid functional or GW methods.[33] The band dispersion along the T→Γ direction that is perpendicular to the MN_2 layers is weaker. It is noteworthy that the band structure portrayed in Figure 7 is qualitatively similar to the one computed for the isostructural compound $CaTaN_2$.[34] In this latter, an additional electron per formula unit occupies the bottom of the conduction band shown in Figure 7. Therefore 2D-metallic properties are envisioned for $CaTaN_2$ whereas the $AEMN_2$ (M=Ti, Zr, Hf) compounds in the α-$NaFeO_2$ structure-type are expected to behave as semiconductors or semimetals according to DFT calculations. The alkaline-earth contribution to the occupied levels is very small in both cases. This suggests that a stronger more covalent interaction occurs in bonds within the MN_2 layers but that ionic bonding exists between the MN_2 layers and the Sr sheets (i.e. $Sr^{2+}(Ca^{2+})[MN_2]^{2-}$). Similar band structures are observed for the α-$NaFeO_2$-type variants of $BaMN_2$ (M = Ti, Zr, Hf) and $CaTiN_2$, suggesting that the bonding in these compounds is similar to that computed for the hypothetical $SrTiN_2$ phase.

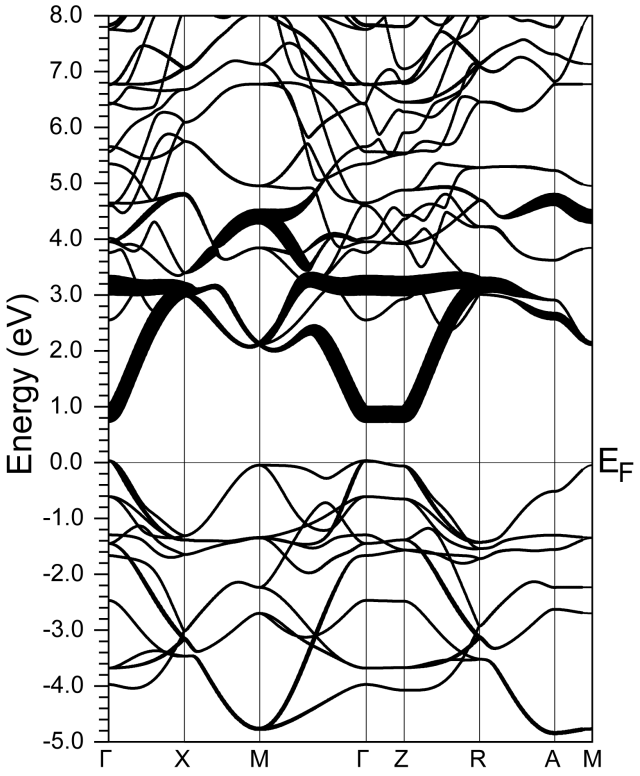

Figure 5. Band structure of $SrTiN_2$ with the $KCoO_2$ structure-type. Γ = (0, 0, 0), X = (0, ½, 0), M = (½, ½, 0), Z = (0, 0, ½), R = (0, ½, ½), and A = (½, ½, ½) in units of the reciprocal lattice vectors. The amount of Ti $3d_{xy}$ character is shown in the band structure by the width of the lines. The Fermi energy level is set at 0 eV.

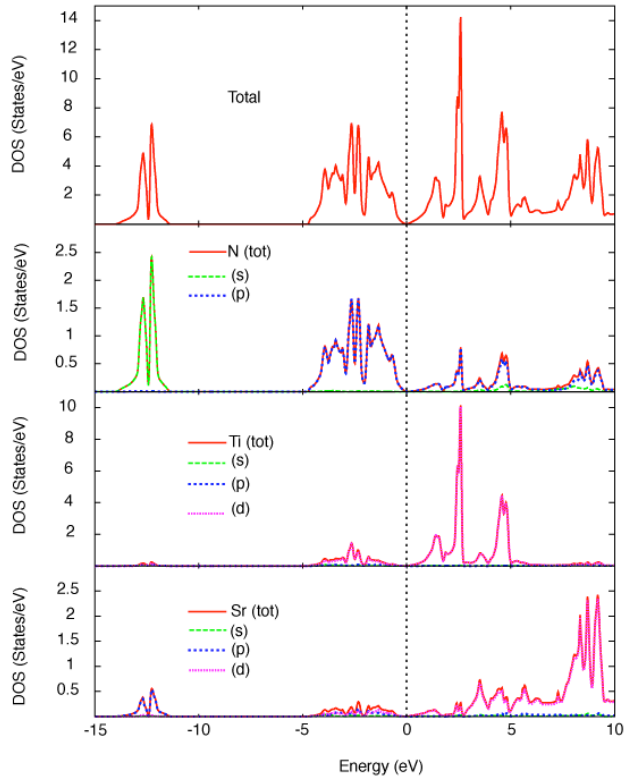

Figure 6. PDOS and DOS of $SrTiN_2$ with the hypothetical α-$NaFeO_2$ structure-type. The Fermi energy level is set at 0 eV.

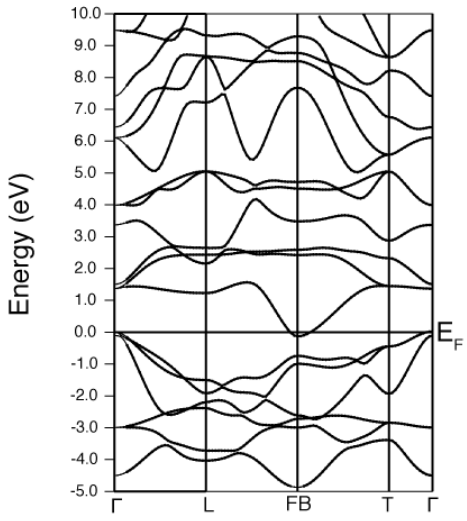

Figure 7. Band structure of $SrTiN_2$ with the hypothetical α-$NaFeO_2$ structure-type. Γ = (0, 0, 0), L = (0, ½, 0), FB = (0, ½, ½), and T = (½, ½, ½) in units of the reciprocal lattice vectors. The Fermi energy level is set at 0 eV.

Conclusions

We have examined the thermodynamics, structural features and electronic properties of the layered group 4 metal ternary nitrides *AEM*N_2 when adopting both the $KCoO_2$ and α-$NaFeO_2$ structure-types within density-functional theory. Considering that compounds with both structure-types are isoelectronic, evidently the *AE*:*M* atomic (ionic) radius ratio is the most important criterion in one structure being imposed over the other. We find that a majority is more stable with the $KCoO_2$ structure-type in which *M* is coordinated by nitrogen in a square-based pyramidal geometry.

Strong interactions occur in both arrangements not only between nitrogen and transition metal atoms, but also between nitrogen and alkaline-earth metal atoms in and between the layers. Calculations show that *AEM*N_2 compounds adopting the tetragonal structure-type $KCoO_2$ are semiconducting with band gaps of approximately 1 eV. By contrast, small band gap conducting and even semi-metallic behaviors are computed for the equivalent compounds when adopting the hexagonal α-$NaFeO_2$ structure-type.

Experimental section

DFT calculations were performed using the WIEN2k program package.[35] The exchange-correlation interaction was treated within the generalized gradient approximation (GGA) of Perdew, Burke, and Ernzerhof.[36] The muffin tin radii (R_{MT}) were chosen small enough to avoid overlapping during the optimization process. A plane wave cutoff corresponding to $R_{MT}K_{max} = 8$ was used, and the radial wavefunctions inside the non-overlapping muffin-tin spheres surrounding the atoms were expanded up to $l_{max} = 12$. The charge density was Fourier expanded up to $G_{max} = 16Å^{-1}$. Total energy convergence was achieved with respect to the Brillouin zone (BZ) integration using a mesh of 500 *k*-points. This generated 30 and 44 k-points in the irreducible Brillouin zone (IRBZ) for compounds in the $KCoO_2$ and α-$NaFeO_2$ structure-type respectively.

Combining *AE* = Ca, Sr, Ba and *M* = Ti, Zr, Hf generates 9 ternary *AEM*N_2 compounds, the structures of which were optimized and analyzed both with the $KCoO_2$ and α-$NaFeO_2$ structure-types. Optimization was obtained by minimizing the total energies of their primitive cells as a function of volume according to Birch-Murnaghan's equation of state:[37, 38]

$$E(V) = E_0 + 9V_0B_0/16\,[(X^2 - 1)^3 B_0' + (X^2 - 1)^2 (6 - 4X^2)]$$

where V_0 represents the equilibrium volume, B_0 the bulk modulus, B_0' the bulk modulus pressure derivative, E_0 the equilibrium energy and $X = (V_0/V)^{1/3}$.

Acknowledgements

The FP7 Marie Curie Initial Training Network FUnctional Nitrides for Energy Applications (FUNEA, European Project No. 264873) is gratefully acknowledged for financial support of this research and a doctoral fellowship for O. E. This work was

granted access to the HPC resources of CINES under allocation 2011-[scr6170] made by GENCI (Grand Equipement National de Calcul Intensif).

Notes and references

[a] Institut des Sciences Chimiques de Rennes, UMR 6226 CNRS - Université de Rennes 1 - Ecole Nationale Supérieure de Chimie de Rennes, F-35708 Rennes Cedex 7, France.
[b] WestCHEM, School of Chemistry, University of Glasgow, Glasgow G12 8QQ, United Kingdom.

1 F. J. DiSalvo, *Science*, 1990, **247**, 649.
2 W. Schnick, *Angew. Chem. Int. Ed.*, 1993, **32**, 806.
3 W. Schnick and H. Huppertz, *Chem.--Eur. J.*, 1997, **3**, 679.
4 N. E. Brese and M. O'Keeffe, *Struct. Bonding*, 1992, **79**, 307.
5 F. J. DiSalvo and S. J. Clarke, *Curr. Opin. Solid State Mater. Sci.*, 1996, **1**, 241.
6 D. H. Gregory, *Dalton Trans*. 1999, 259.
7 R. Kniep, *Pure Appl. Chem*., 1997, **69**, 185.
8 R. Niewa and H. Jacobs, *Chem. Rev.*, 1996, **96**, 2053.
9 A. Simon, *Coord. Chem. Rev.*, 1997, **163**, 253.
10 D. H. Gregory, *Coord. Chem. Rev.*, 2001, **215**, 301.
11 D. A. Headspith and M. G. Francesconi, *Top. Catal.*, 2009, **52**, 1611.
12 L. Hongmei, W. Haiyan, Z. Guifu, B. Eve, M. M. Thomas, K. B. Anthony and J. Quanxi, *Trans. Electr. Electron. Mater.*, 2010, **11**, 54.
13 J. M. Cameron, R. W. Hughes, Y. Zhao and D. H. Gregory, *Chem. Soc. Rev.*, 2011, **40**, 4099.
14 N. Tapia-Ruiz, M. Segalés and D. H. Gregory, *Coord. Chem. Rev.*, 2013, **257**, 1978.
15 D. A. Vennos, M. E. Badding and F. J. DiSalvo, *Inorg. Chem*., 1990, **29**, 4059.
16 D. A. Vennos and F. J. DiSalvo, *J. Solid State Chem*., 1992, **98**, 318.
17 M. G. Barker, M. J. Begley, P. P. Edwards, D. H. Gregory and S. E. Smith, *Dalton Trans.*, 1996, 1.
18 G. Cordier, P. Höhn, R. Kniep and A. Rabenau, *Z. Anorg. Allg. Chem.*, 1990, **591**, 58.
19 D. H. Gregory, M. G. Barker, P. P. Edwards and D. J. Siddons, *Inorg. Chem*., 1995, **34**, 5195.
20 M. Y. Chen and F. J. DiSalvo, *J. Solid. State Chem*., 1990, **88**, 459.
21 D. H. Gregory, M. G. Barker, P. P. Edwards and D. J. Siddons, *Inorg. Chem*., 1995, **34**, 3912.
22 V. Balbarin, R. B. Van-Dover and F. J. DiSalvo, *J. Phys. Chem.*, 1996, **57**, 1919.
23 D. J. Singh, *Phys. Rev. B: Condens. Matter Mater. Phys.*, 1992, 46, 9332.
24 K. S. Weil and P. N. Kumta, *J. Solid. State Chem*., 1997, **128**, 185.
25 D. H. Gregory, M. G. Barker, P. P. Edwards and D. J. Siddons, *Inorg. Chem.*, 1996, **35**, 7608.
26 D. H. Gregory, M. G. Barker, P. P. Edwards, M. Slaski and D. J. Siddons, *J. Solid. State Chem*., 1998, **137**, 62.
27 D. H. Gregory, M. G. Barker, P. P. Edwards and D. J. Siddons, *Inorg. Chem*., 1998, **37**, 3775.
28 G. Farault, R. Gautier, C. F. Baker, A. Bowman and D. H. Gregory, *Chem. Mater*., 2003, **15**, 3922.
29 WebElements: the periodic table on the WWW [http://www.webelements.com/].
30 A. Kaur, E. R. Ylvisaker, Y. Li, G. Galli and W. E. Pickett, *Phys. Rev. B: Condens. Matter Mater. Phys.*, 2010, **82**, 155125.
31 O. Seeger, M. Hofmann and J. Strähle, *Z. Anorg. Allg. Chem*., 1994, **620**, 2008.
32 I. Ohkubo, T. Mori, *Chem. Mater*. 2014, **26**, 2532.
33 F. Tran and P. Blaha, *Phys. Rev. Lett.*, 2009, **102**, 226401.
34 J. M. Oliva, R. Weht, P. Ordejon and E. Canadell, *Phys. Rev. B: Condens. Matter Mater. Phys.*, 2000, **62**, 1512.
35 P. Blaha, K. H. Schwarz, G. K. H. Madsen, D. Kvasnicka and J. Luitz, *WIEN2k An Augmented Plane Wave + Local Orbitals Program for Calculating Crystal Properties*, revised edition WIEN2k 11.1 (Release 30.03.2011, http://www.wien2k.at)
36 J. P. Perdew, K. Burke and M. Ernzerhof, *Phys. Rev. Lett*., 1996, **77**, 3865.
37 F. Birch, *Phys. Rev*., 1947, **71**, 809.
38 F. D. Murnaghan, *Proc. Nat. Acad. Sci*., 1944, **30**, 244.

Table of contents entry

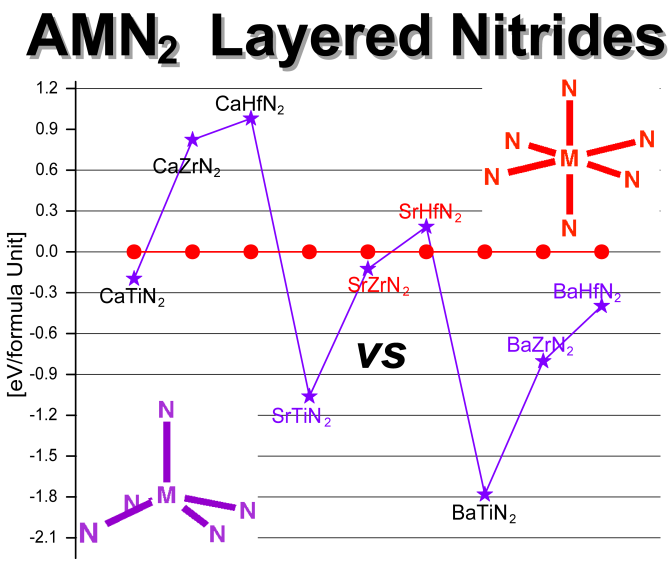

Synopsis TOC. DFT calculations allow the rationalization of the structural and electronic properties of $AEMN_2$ compounds whether the metals adopt an octahedral or a square-based pyramidal environment of nitrogen atoms.